④

RADC-TR-89-102
Final Technical Report
August 1989

AD-A215 026

ELECTRON-BEAM PHASE-ONLY SPATIAL LIGHT MODULATOR FOR MATCHED FILTERING

Optron Systems, Inc.

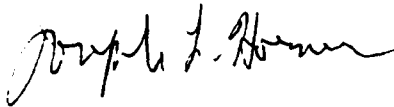Cardinal Warde and Robert L. Hillman

DTIC
S ELECTE
NOV 24 1989
B D

ROME AIR DEVELOPMENT CENTER
Air Force Systems Command
Griffiss Air Force Base, NY 13441-5700

89 11 21 130

This report has been reviewed by the RADC Public Affairs Division (PA)
and is releasable to the National Technical Information Service (NTIS). At
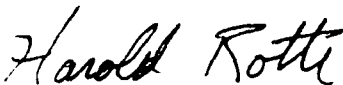NTIS it will be releasable to the general public, including foreign nations.

RADC-TR-89-102 has been reviewed and is approved for publication.
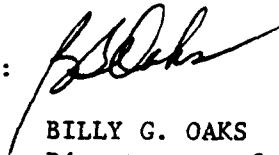

APPROVED: *[signature]*

JOSEPH L. HORNER
Project Engineer

APPROVED: *[signature]*

HAROLD ROTH
Directorate of Solid State Sciences

FOR THE COMMANDER: *[signature]*

BILLY G. OAKS
Directorate of Plans & Programs

REPORT DOCUMENTATION PAGE		*Form Approved* *OMB No. 0704-0188*

1a. REPORT SECURITY CLASSIFICATION UNCLASSIFIED		1b. RESTRICTIVE MARKINGS N/A		
2a. SECURITY CLASSIFICATION AUTHORITY N/A		3. DISTRIBUTION / AVAILABILITY OF REPORT Approved for public release;		
2b. DECLASSIFICATION / DOWNGRADING SCHEDULE N/A		distribution unlimited.		
4. PERFORMING ORGANIZATION REPORT NUMBER(S) N/A		5. MONITORING ORGANIZATION REPORT NUMBER(S) RADC-TR-89-102		
6a. NAME OF PERFORMING ORGANIZATION Optron Systems, Inc.	6b. OFFICE SYMBOL *(If applicable)* N/A	7a. NAME OF MONITORING ORGANIZATION Rome Air Development Center (ESCC)		
6c. ADDRESS *(City, State, and ZIP Code)* 3 Preston Court Bedford MA 01730		7b. ADDRESS *(City, State, and ZIP Code)* Hanscom AFB MA 01731-5000		
8a. NAME OF FUNDING / SPONSORING ORGANIZATION Rome Air Development Center	8b. OFFICE SYMBOL *(If applicable)* ESO	9. PROCUREMENT INSTRUMENT IDENTIFICATION NUMBER F19628-86-C-0186		
8c. ADDRESS *(City, State, and ZIP Code)* Hanscom AFB MA 01731-5000		10. SOURCE OF FUNDING NUMBERS		

		PROGRAM ELEMENT NO. 61102F	PROJECT NO 2305	TASK NO J7	WORK UNIT ACCESSION NO 29

11. TITLE *(Include Security Classification)*

ELECTRON-BEAM PHASE-ONLY SPATIAL LIGHT MODULATOR FOR MATCHED FILTERING

12. PERSONAL AUTHOR(S)
Cardinal Warde, Robert L. Hillman

13a. TYPE OF REPORT Final	13b. TIME COVERED FROM Aug 87 TO Sep 88	14. DATE OF REPORT *(Year, Month, Day)* August 1989	15. PAGE COUNT 36

16. SUPPLEMENTARY NOTATION

N/A

17.	COSATI CODES		18. SUBJECT TERMS *(Continue on reverse if necessary and identify by block number)*
FIELD	GROUP	SUB-GROUP	Correlation, Pattern Recognition, Phase-Only Filtering
17	08		

19. ABSTRACT *(Continue on reverse if necessary and identify by block number)*

A vacuum demountable electron-beam addressed LiNbO₃ crystal spatial light modulator was
designed, fabricated, and tested. The device works in a phase-only mode, capable of
being placed in the filter plane of a coherent optical correlator. The measured per-
formance parameters were: spatial resolution-2 lines/mm; contrast ratio - 20:1; phase
dynamic range 5 pi, and storage time - 5 minutes. A theoretical resolution of 10 lines/
mm would be possible with an improved electron gun assembly.

20. DISTRIBUTION / AVAILABILITY OF ABSTRACT ☒ UNCLASSIFIED/UNLIMITED ☐ SAME AS RPT ☐ DTIC USERS	21. ABSTRACT SECURITY CLASSIFICATION UNCLASSIFIED	
22a. NAME OF RESPONSIBLE INDIVIDUAL Joseph L. Horner	22b. TELEPHONE *(Include Area Code)* (617) 377-3841	22c. OFFICE SYMBOL RADC (ESOC)

DD Form 1473, JUN 86   *Previous editions are obsolete.*

TABLE OF CONTENTS

I. BACKGROUND AND PROGRAM GOALS

The use of coherent optical processors for pattern recognition has a rich history of applications due primarily to the work of Vander Lugt[1] who first demonstrated the applicability of holography in facilitating the synthesis of complex spatial filters. In particular, related techniques have subsequently been employed by numerous authors to generate classical matched filters (CMFs) for use in pattern recognition applications.[2-6] The classical matched filter is a fully complex filter that spatially modulates both the amplitude and phase of light passing through it, and it gives reasonably high signal-to-noise ratio when used in a coherent optical correlator.

Recently, however, Horner and Gianino[7,8] proposed the use of phase-only matched filters for pattern recognition. Using computer simulation to compare the performance of a phase-only filter with the corresponding classical matched filter, these authors concluded that the phase-only filter has several advantages over the classical matched filter: (1) the optical efficiency of the phase-only filter is always significantly higher than that of the classical matched filter, (2) the absolute peak energy in the correlation plane is many times higher for the phase-only filter than for the classical matched filter and (3) the phase-only offers higher peak-to-side lobe ratio than the classical matched filter and in fact is optimum.[16]

Additional characteristics of the phase-only filter include: (1) considerably smaller data storage requirements compared to other correlation filters, (2) implementable on several currently available spatial light modulators, (3) better discrimination to out-of-class targets.[7] Therefore, the phase-only correlation filter may be the best choice in applications where low input optical power to the correlator is crucial or where a high level of discrimination is needed.

The research goals were to: (1) develop and characterize a low-cost, near real-time, phase-only spatial light modulator that will serve as a

3

programmable recording medium for the synthesis of phase-only 2-D objects and filters from 1-D electrical signals, and (2) to demonstrate and explore the limitations of low-resolution phase-only filtering and pattern recognition. The specific spatial light modulator on which the development work focused is the vacuum demountable electron-beam addressed $LiNbO_3$ spatial phase modulator.

II. ELECTRON-BEAM ADDRESSED SPATIAL PHASE MODULATOR

Device Description

A schematic of the vacuum-demountable electron-beam addressed $LiNbO_3$ spatial phase modulator and associated readout optics appears in Fig. 1. In its current configuration the device consists of an electron gun, a stray electron collecting ring, G_1, a control grid, G_2, and a thin $LiNbO_3$ electrooptic crystal. The crystal is coated on one surface with a dielectric mirror, and on the other side with a transparent electrode, A.
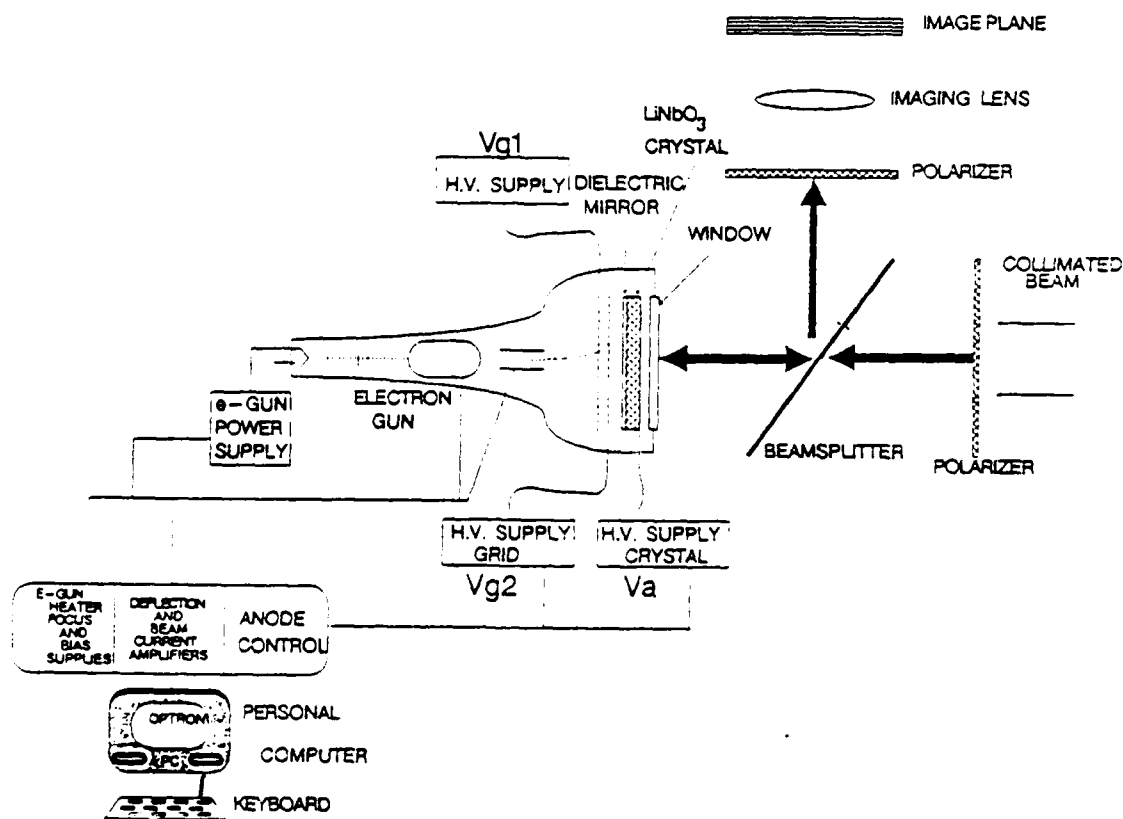

Fig. 1.   Vacuum-demountable $LiNbO_3$ spatial phase modulator.

4

In operation, the electron gun produces a well-focused electron beam that is raster or vector scanned across the dielectric mirror. The desired spatial distribution of charge can be synthesized in three different ways. The application of a time-varying voltage waveform to: (1) the control grid, V_{g2}, (2) the transparent electrode on the crystal, V_a, or (3) the cathode of the electon gun, V_k. This waveform is synchronized with the beam scan so that the surface charge density accumulated at each beam location (by the deposition or removal of elecrons) is proportional to the phase modulation desired there. Through the linear electrooptic effect, the resulting longitudinal electric field established in the electrooptic material spatially varies the refractive index of the modulator material. Thus the coherent readout beam which makes a double pass through the electrooptic plate is phase modulated.

Optimally, the electrooptic material chosen should: (1) require minimal surface charge density to achieve a given phase modulation, (2) exhibit low halfwave voltage (the voltage across the crystal required to change the crystal's optical path length by 0.5 waves), (3) exhibit high dielectric breakdown strength so that several waves of phase modulation are achievable, (4) be vacuum compatible and (5) be capable of being polished into thin wafers. $LiNbO_3$ has several of these characteristics.

Principles of Operation

The specific process described above for the first two of the three mechanisms for the deposition and removal of electrons from the dielectric mirror is referred to as the grid stabilized mode of operation. The mechanism used in the third is the cathode-stabilized mode of operation. The grid stabilized mode exploits the secondary electron emission characteristics of the mirror in such a manner that the voltage of the mirror surface is automatically driven towards an equilibrium value which is close to the instantaneous grid voltage. The requirement for this mode of operation is that the secondary electron emission characteristic of the mirror exceed unity for incident electron energy. The cathode-stabilized mode of operation is achieved when the electron energies are such that the

5

secondary electron emission coefficient is less than unity. In this case, the surface of the crystal will charge to the cathode potential, and removal of charge requires a second flood gun operating at the appropriate potential for electron removal by secondary emission.

Figure 2 is an illustration of the secondary electron emission characteristics of an insulating surface such as the dielectric mirror. The coefficient $\delta(E_p)$ is a characteristic of the surface material and represents the ratio of the number of emitted secondary electrons to the number of primary electrons incident on the uncharged surface, where E_p is the energy of the primary electrons. For insulators, the first crossover energy E_1 (at which $\delta = 1$) is typically 20-50 eV and the second crossover energy is on the order of many thousands of eV. The secondary electron emission curve for an insulator generally has a peak value between 1.5 and 25. The energy of the emitted electrons, E_s, is generally less than 50 eV and has little dependence on E_p.[9]
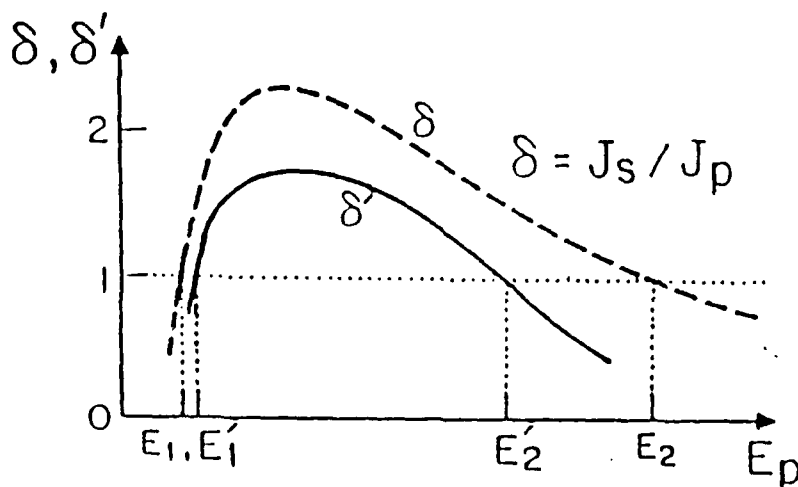
Fig. 2. Secondary emission characteristic of an insulating target.

When the surface is charged, the intrinsic curve $\delta(E_p)$ is no longer valid. If, in addition, the secondary electrons emitted from the surface are collected, it becomes expedient to define a collected secondary electron emission coefficient $\delta'(E_p)$ as shown in Fig. 2, which is the ratio of the number of electrons collected to the number of electrons incident on the insulator surface. The result is a family of curves $\delta'(E_p)$ which depends not only on the material characteristics and the primary electron energy, but

6

also on the collection geometry and the potential differences between the collector and the insulator surface. It is the manipulation of $\delta'(E_p)$ which permits electrons to be removed from or added to the dielectric mirror during grid stabilized mode operation.

The principle of the grid stabilized mode is illustrated in Fig. 3. If, at a given beam location, the previously established mirror surface voltage is more positive than the currently applied grid voltage (Fig. 3a) electrons are attracted to the mirror and the voltage of the mirror is reduced. When the given location requires a more positive potential than the previously established value, (Fig. 3b) primary electrons with kinetic energies greater than the mirror-to-grid retarding field will penetrate to the mirror and liberate secondary electrons which will then be collected by the grid.
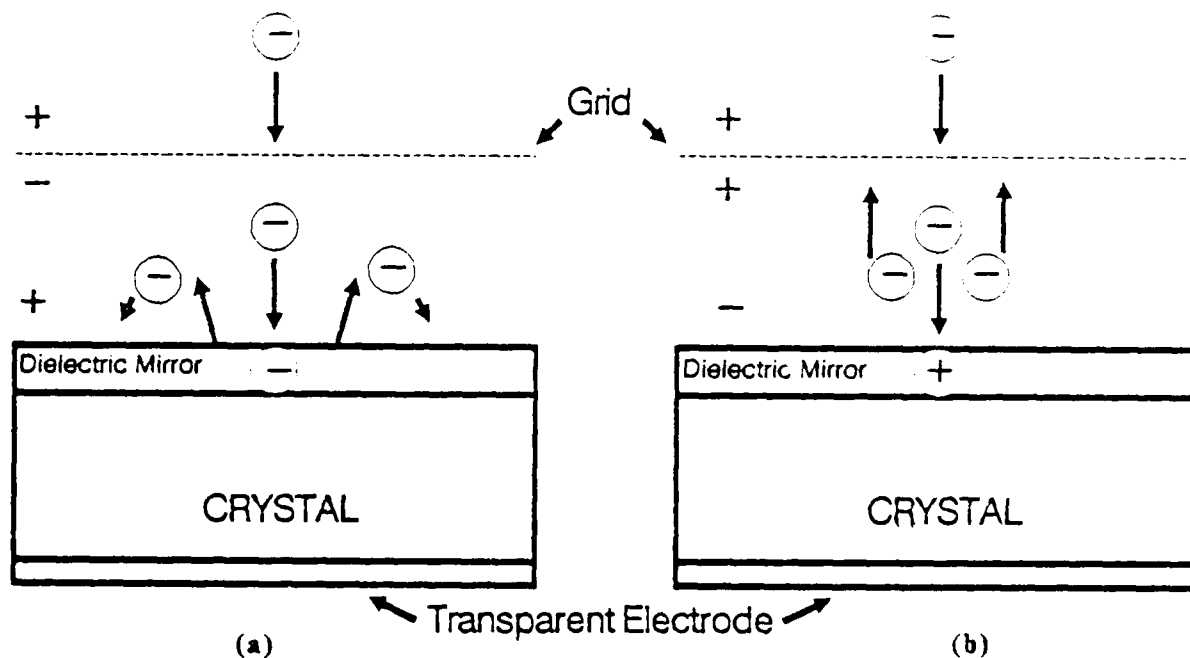

Fig. 3.   Grid Stabilized Mode. (a) The surface voltage is lowered to the grid potential by electron deposition. (b) The surface voltage is raised to the grid voltage by secondary emission.

III. RESEARCH ACCOMPLISHMENTS

Electron gun and vacuum-demountable test cell

A specialized vacuum test cell was designed and fabricated for the purpose

of developing and testing the modulators. This vacuum cell has a port for mounting the electron gun on axis, an off-axis window for viewing the anode during testing, and a readout window directly opposite the electron gun port. The cell is mounted on an optical table and connected to a large-capacity ion pump for rapid turnaround time and very high vacuum.

Electron guns from Cliftronics, Tektronix, Kimball physics and most recently Teltron have been investigated in an effort to locate an electron gun with spot sizes less than $50\mu m$ and beam current of greater than $1\mu A$ for low acceleration potentials. The majority of the guns considered had oxide cathodes which must be activated. Once activated a constant vacuum of 10^{-7} Torr or better must be maintained. Most of the work reported herein was carried out with the Tektronix guns. The Tektronix guns had been advertised to have a spot size of approximately $75\mu m$ with an associated beam current of $10\mu A$ for a cathode potential of -5.6kV. The operating cathode potential for our device was -1.5kV. Operating at this low potential seriously expanded the beam spot and reduced the amount of current delivered to the anode of the device (see Fig. 4). Minimal success was achieved in the reduction of the beam profile using the Tektronix control box. Currents of 2-3 μA and line widths of $350\mu m$ were witnessed for $V_k = -1.5kV$.

Fig. 4.   The image above has been written on the LiNbO$_3$ crystal with the unaltered Tektronix electron beam spot. The cathode potential, V_k = -1.5kV.

Toward the end of the program, we were able to procure and sucessfully operate a vidicon-type gun for spatial light modulator purposes. This gun, unlike the Tektronix gun, is magnetically focused and its spot size is approximately $100\mu m$ with current of $1-2\mu A$ at cathode potential of -200V. Future work will involve the use of such high resolution guns.

8

Measurement of electron gun spot size

Measurement of the Tektronix electron gun spot size for a variety of conditions was achieved by using a P-20-phosphor window as an anode. The current levels, acceleration potentials, and astigmator potentials used were similar to those used with the crystal systems. The minimum spot size, for a given set of conditions, was determined. The spot diameter on the crystal was slightly larger than that observed with the phosphor anode. This is because charge builds up on the insulative crystal surface during operation whereas charge bleeds quickly away on the phosphor anode.

Minimization of electron gun spot size

Minimization of the electron gun spot diameter was achieved by adjusting the electron current level, the acceleration potential, the electron beam astigmatism, and the exposure time of the primary electrons. Using a combination of these parameters we were able to reduce the spot size to the point where it was beyond the theoretical resolution limit of the $330\mu m$ thick $LiNbO_3$ crystal that was available. However, the current densities were too low to achieve effective modulation within a reasonable time.

The most productive measure for spot diameter reduction and effective modulation was the introduction of an astigmatism to the electron gun spot. Line charge generation was best accomplished via the adjustment of the potentials for the astigmator electrodes of the Tektronix electron gun. The resultant line charge distributions were narrower than those generated with the unaltered electron beam. The minimum line width achieved at $V_k = -1.5kV$ was $350\mu m$, at a current density of about $100nA/cm^2$.

Measurement of electron gun current

Determining the relationship between the current measured at the imaging grid, G_2, and the electron current density reaching the crystal surface was of interest because of its implications on the spot size and frame rate. In order to determine this a phosphor window with an ITO backcoat was

substituted in place of the crystal. The layout of the anode is pictured in Fig. 5. The electrode G_1 functions as a mask keeping stray electrons which fall outside of the active crystal or phosphor area from being collected by any subsequent electrodes. G_1 serves as a known aperture through which the electron current is allowed to flow.
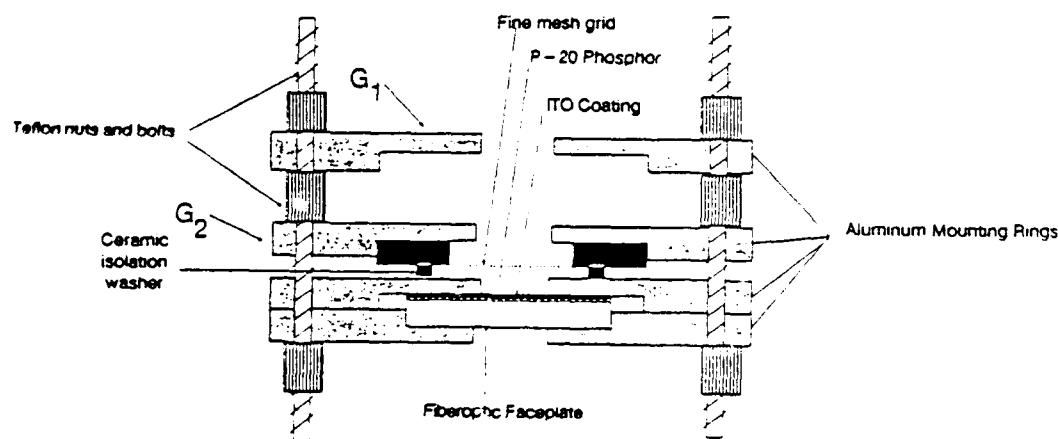

Fig. 5. Anode configuration used to determine current densities delivered by the electron guns. This assembly is attached to the test cell.

Through visual observation of the beam profile as a function of preacceleration, focus, and x-y deflection voltages, a flood electron-beam which covers 50% of the 3 cm^2 phosphor window was obtained. It was found that for V_K = -1.5kV the most negatively biased element of the G_2 or $G_{phosphor}$ electrodes yielded electrons. This was noted when the sign of the current measured at that electrode indicated that the electrode was acting as a source of electrons rather than a sink. Presently the only mechanism to account for this observation is the secondary emission of electrons from the most negative electrode to the surrounding more positive surfaces. If this same phenomenon occurs when the crystal is present it will contribute to resolution loss with high density grids. This is because secondary electrons emitted from the grid will fall onto crystal surface, introducing noise in the image. Figure 6b indicates that the flood electron gun was capable of delivering 1.1µA of cu. ent across a 2cm diameter phosphor window. This implies that for i_{g2} = +150nA, the current density delivered by the flood gun, $J_{flood-gun}$ = 362nA/cm^2. The same experiment was done with the Tektronix electron gun (Fig. 6b). In this case we are observing a pencil beam and for +10nA at the G_2, we measured -300nA at the $G_{phosphor}$ electrode.

10

$J_{Tektronix} \approx 100nA/cm^2$. The current values were taken in the region where it appears that the current is saturating to its maximum absolute value. The grid material being used is nickel. Theoretically $\delta_{nickel} < 1$ for all electron energies of interest. Subsequent processing of the nickel grid material may have changed this property.
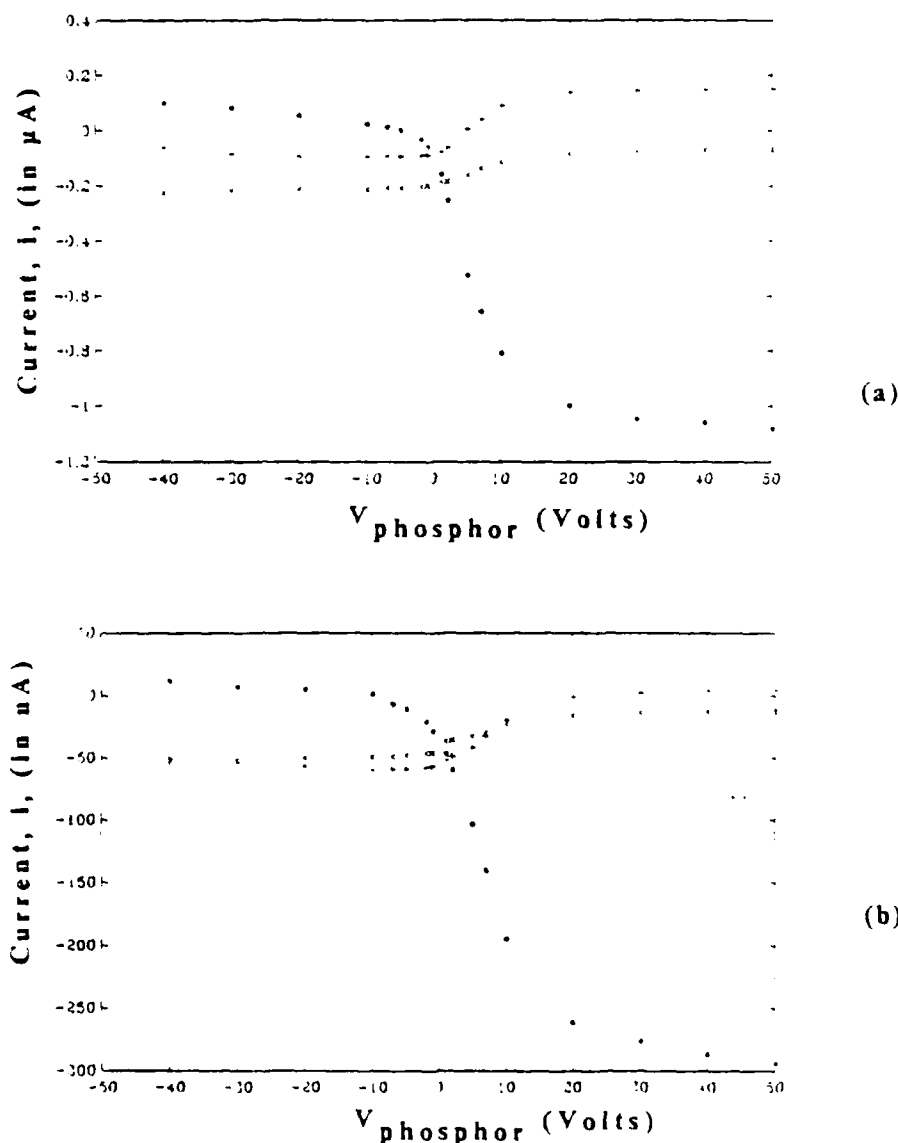

(a)

(b)

Fig. 6.   (a) Plot of flood gun current at G_1, G_2, $G_{phosphor}$ as $V_{phosphor}$ is increased. (b) Plot of Tektronix gun current as G_1, G_2, $G_{phosphor}$ as $V_{phosphor}$ is increased. '*','x','+' represent data points for $I_{phosphor}$, i_{g1}, and i_{g2} respectively where i represents current.

Modulator Evaluation Procedures

The primary goal of the research was to construct a vacuum demountable version of the e-beam addressed spatial phase modulator with a z-cut $LiNbO_3$ crystal. Once fabricated this device can be used for a number of applications. Towards this end, a 55^0-cut $LiNbO_3$ crystal was first used to characterize and develop the vacuum-demountable e-gun system and anode assembly in which the z-cut crystal would later be placed. This approach revealed many problems that were unanticipated at program inception. Due to the simplicity of the readout scheme for the 55^0-cut $LiNbO_3$ crystal the optimum operating voltages for deposition and depletion of electrons from the mirrored surface of the crystal were readily obtainable. The reduction of stress induced birefringence, the performance of uniformity tests, as well as the determination of the differential phase dynamic range, were also more efficiently achieved.

Test procedures for characterizing spatial phase modulators were developed. The optical readout of the $LiNbO_3$ crystal was accomplished with a collimated He-Ne laser beam (633 nm wavelength). The crystal was placed between two crossed polarizers when the amplitude modulation was desired. When phase - only modulation was required the input polarizer and output analyzer was aligned parallel to one or the other crystal axes. The pattern written onto the crystal was imaged by means of lenses onto the output image plane. When performing spatial resolution and framing speed measurements, a pinhole aperture in conjunction with a photomultiplier tube mounted on a motorized translation stage was used to scan the image plane. The PMT output signal was monitored by a lock-in amplifier synchronized to the frequency of the chopped input radiation to improve the signal-to-noise ratio. The amplifier output was attached to a chart recorder or oscilloscope or a digital-to-analog converter. Procedures were developed for characterizing the resolution, write/erase time, secondary electron emission characteristics of the dielectric mirror and grid material, storage time, uniformity of response, intensity contrast ratio, differential phase dynamic range and absolute phase dynamic range. Concomitant with test procedures, a data

acquisition system was conceived and debugged for performance verification, analysis, and optimization. It is continuosly being modified and enhanced to allow greater efficiency in the development effort fo electron-beam addressed spatial light modulators.

CTP/LiNbO$_3$ Anode Assembly

Three SLM anode designs were evaluated, two have shown feasibility. Figure 7 shows the first sucessful anode assembly incorporated into an electron gun test cell for evaluation. This anode assembly employed a charge transfer plate (CTP). The motivation for exploring this anode assembly is that the CTP which is a leak-tight window consisting of hundreds of thousands of conducting filaments, transfers charge from the inside of the electron gun envelope to the outside. Thus the crystal can be replaced outside the vacuum, thereby simplifying fabrication.
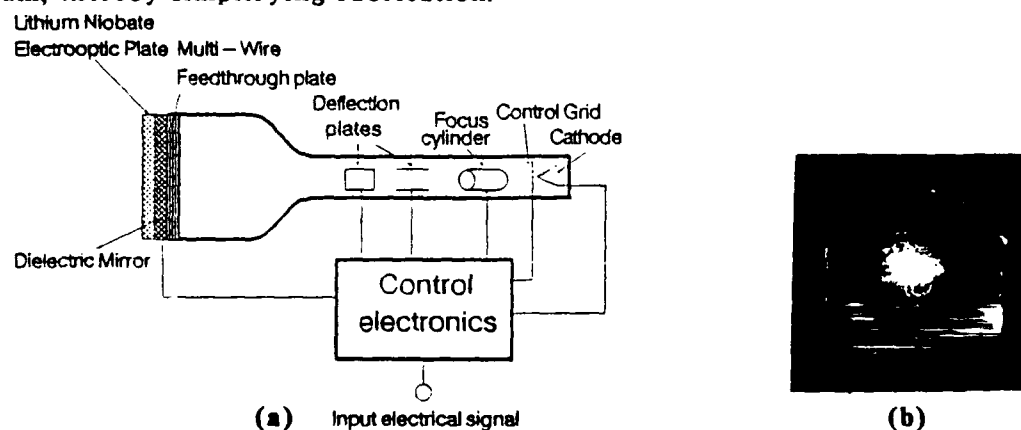
Fig. 7.   (a) Schematic drawing of vacuum-demountable LiNbO$_3$/CTP anode. The envelope represents the evacuated test cell, (b) Output of 55^0-cut LiNbO$_3$/CTP combination with electron gun dwelling in one spot.

The construction of the device with the e-gun and CTP/LiNbO$_3$ anode assembly is illustrated in Fig. 7a. An intensity output distribution reflecting the electron gun spot is illustrated in Fig. 7b. This anode assembly exhibited a storage time of 3-5 seconds. The optical reflectance of a polished CTP has been determined to be 50%. With the electron gun cathode biased at -4kV, a grid voltage of +2kV, and V$_a$ biased at +4kV, amplitude modulation of He-Ne laser light was achieved. The acceleration of the electrons impinging onto the CTP in combination with the secondary emission characteristics of the

13

CTP relegated operation of the device to the electron deposition mode. That this was true was bourne out by other studies which concluded that $\delta_{CTP} \lesssim 1$, for all electron energies. Removal of charge was accomplished via the leakage currents that exist in the above configuration. No further device evalution was done with this combination because no suitable mechanism for effecting contact between the CTP and the $LiNbO_3$ crystal was found.

Several agents for bonding $LiNbO_3$ to CTP were investigated. Results of this study are incomplete as there exist a large number of resins. Resin testing was suspended to proceed with some of the more fundamental issues of the modulator development program. Those resins which were evaluated have been found to be unsatisfactory because their physical properties are incompatible with $LiNbO_3$. The thermal coefficients of expansion, surface and bulk conductivities, and viscosity requirements were incompatible for the resin systems tested. The evaluation of Norland Optical, Space Environmental Labs Vac-seal, and other resins remains to be completed.

Directly-Addressed $LiNbO_3$ Anode Assembly

In an effort to resolve more fundamental issues, the focus of the project became the construction of the vacuum demountable electron-beam addressed phase-only spatial light modulator without the CTP. This anode assembly is illustrated in Fig. 8.
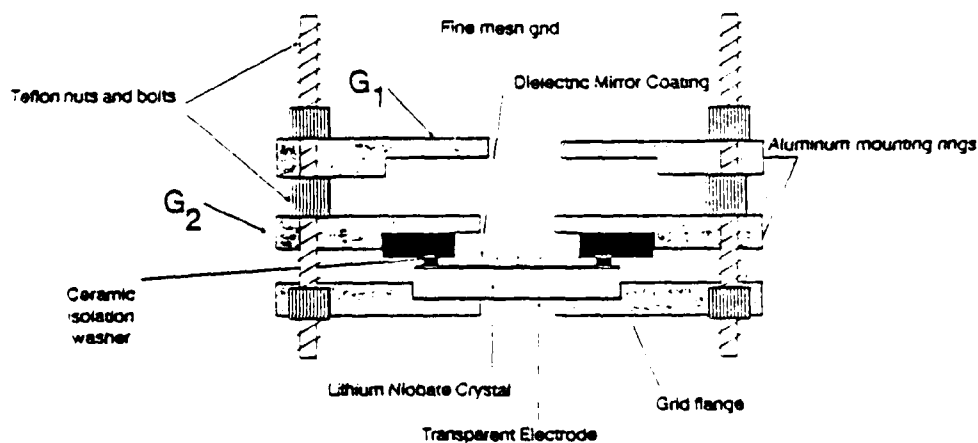

Fig. 8. Anode Assembly of the Direct E-beam Addressed $LiNbO_3$ Phase Modulator. This assembly is attached to the door of the test cell.

Crystals coated with a ZrO_2/SiO_2 dielectric mirror were well suited for phase-only spatial light modulation. In comparison with earlier crystals which were coated with ThF_4/SbS_3, the crystal coated with the ZrO_2/SiO_2 dielectric mirror retained charge patterns longer. Several other performance parameters also improved, specifically, output uniformity, resolution, and secondary emission.

Mechanical fixturing was designed (see Fig. 8) which allows the crystal to be mounted relatively stress free in the vacuum-demountable system. This fixturing effectively reduces the amount of stress induced birefringence. A second circular flange has been included in the design of the electron-beam addressed spatial light modulator. This flange serves as an aperture for primary electrons thereby increasing the accountability of stray electrons when flood electron beam experiments are being performed. It is also useful in reducing the effect of secondary electron redistribution on resolution.

Modulation uniformity was improved by hydrogen firing the grid assembly. Hydrogen firing causes the grid material to shrink providing a taut, uniform grid. The placement of the stretched grid parallel to the crystal surface provides uniform fields for the control of secondary electrons leaving the crystal surface. More important is the fact that the capacitive voltage division across the gap and crystal is uniform over the active area of the device.

An image written on the 55^0-cut crystal using direct addressing with a low-resolution Tektronix electron gun is shown in Fig. 9.

Fig. 9.   Image read out from an electron-beam addressed 55^0-cut $LiNbO_3$ crystal where the electron beam directly addresses the crystal (no CTP). The input polarization is polarized at 45^0 to the x or -y crystallographic axis and the output analyzer is rotated 90^0 with respect to the input polarization.

Device Control Electronics and Computer Interface

Three (3) programmable video generator cards were procured from Lynx Communications through a subcontract. Software to drive the cards was developed at Optron. The cards along with the software are used to operate the control grid and/or anode electrode of the $LiNbO_3$ crystal in addition to the deflection plates of the electron-gun in the electron-beam-addressed phase-only spatial light modulator. The video generator serves as a programmable interface through which a microcomputer can control the spatial light modulator. The generator provides an image memory for storage of up to 64K pixel-write instructions, each consisting of x and y coordinates and an intensity value for the pixel. Using the provided control inputs, the image memory can be divided among an arbitrary number of images. By storing images as a linked list of write instructions, the generator inherently performs vector scanning and thus requires minimal framing time for images. Nevertheless, the generator can, if desired, effect a raster scan if the image to be written is stored as a raster sequence of pixels.

A menu-driven user-interface, as well as a machine emulator have been written and tested to support the hardware described above. The user interface enables the user to: (1) download (write) a specific image file to the modulator in a single-shot or repeating mode; (2) erase the device; (3) adjust the desired overall modulation depth and modulation offset on the readout beam; (4) synchronize device erasure and writing to externally-supplied (TTL-level) triggers; (5) skew the position and adjust the aspect ratio of the modulation pattern across the face of the modulator; (6) add, subtract and multiply image files; (7) automatically pre-correct image files to compensate for any static, non-ideal behavior present in the modulator; (8) vector or raster scan images in memory to the modulator. Thus the generator provides an enormous amount of flexibility for SLM control.

Upon initial delivery, the programmable video generator was first connected to an AT&T PC 6300 and then tested using diagnostic routines written at Optron Systems, Inc. The prototype device was found to have two bugs: a noisy clock line causing erratic data storage and a defective auxiliary

16

clock input. The generator was sent back to the manufacturer and Lynx upon return to Optron the device was tested and found to be in good working condition.

Once assured that the generator was functioning as designed, the system integration process began. The first step was to connect the device to a Tektronics monitor containing an electron gun and drive electronics identical to those to be used in our demountable light modulator. The pixel-write instructions for a series of images to be used as test patterns were then calculated and written to a set of ASCII files on the computer. The generator was loaded with a 128-by-128 image of an annulus, which was sucessfully written to the monitor. Next, the generator image memory was loaded with a series of 18 different 16-by-16 images to be displayed in rapid succession. The generator successfully displayed the 18 images as a sequence of frames simulating motion on the monitor.

LiNbO$_3$ Crystal Storage

The ability to deposit localized charge and have it remain localized, (i.e., storage) improves several of the performance parameters. Device storage depends heavily upon the quality of the dielectric mirror. If the mirror is contaminated by a conductive substance the mobility of surface charge is enhanced. This will manifest itself in the output intensity as blurred images caused by charge migration.

Numerous attempts were made to observe charge storage on several 55^0-cut LiNbO$_3$ crystals coated with ZrO_2/SiO_2. The use of ZrO_2/SiO_2 in this application was no mystery to Optron as the electro-optic plates used in the Microchannel Spatial Light Modulator had been coated with the same material. Unfortunately the vendors that had reliably coated crystals for Optron in the past had quality control problems. In lieu of ZrO_2/SiO_2 dielectric mirrors, ThF_4/SbS_3 dielectric materials were chosen.

Upon first attempts to write a spot of charge to the $ThF_4/SbS_3/LiNbO_3$ device, the electron spot spreads in a matter of 2-3 seconds. To improve upon the storage the crystal was baked in an O_2 rich environment. This

17

oxidizes contaminants and drives out moisture. The result of the bake-out was that storage improved. Images written to this device could be visually discerned for greater than 5 minutes. It was also noticed that storage improved as better vacuum was achieved in the test cell. This indicated that contaminants were being degassed from the dielectric mirror.

The SiO_2/ZrO_2 dielectric materials were chosen for their storage capability, their hardness, and their reflectivity at 6328Å. A vendor was found who could reliably deposit the ZrO_2/SiO_2 dielectric mirror onto the $LiNbO_3$ crystal. In comparison with the ThF_4/SbS_3 dielectrics, ZrO_2 and SiO_2 were superior in all respects. Storage was achieved without requiring that the crystal be baked in an O_2 rich environment. Additionally, the surface damage attributed to the electron bombardment observed with the ThF_4/SbS_3 dielectrics was not evident with the SiO_2/ZrO_2 dielectrics. The deterioration of line charge distributions written to this device after a 90 hour period is recorded in Fig. 10.

| (a) | (b) | (c) |
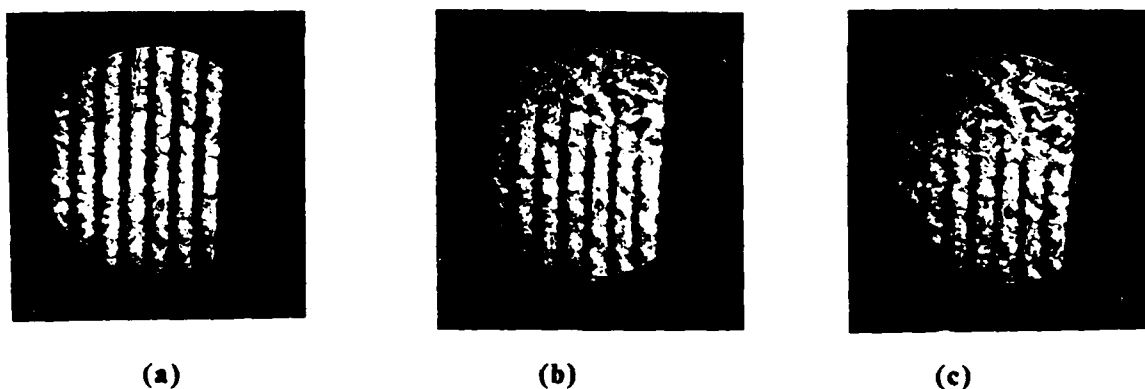
Fig. 10   Elapsed time photographs of ZrO_2/SiO_2 coated $LiNbO_3$ crystal. (a) t = 0 hrs., (b) t = 75 hrs., (c) t = 90 hrs.

Static Crystal Response

In order to write complicated images onto the modulator the voltage/readout intensity modulation transfer characteristic had to be obtained. Knowledge of this transfer function allows one to determine operating voltages for the device, thereby permitting one to take full advantage of the three possible modes of operation. The electron flood beam was focused onto the crystal as V_a was increased to more positive values. Several runs were

attempted. In general, the shapes of the curves agreed from run to run on a given crystal. The typical transfer characteristic is illustrated in Fig. 11. Incongruity in the data from trial to trial given the same crystal was attributed to thermal drift. The shape of the transfer curve contracts, expands, and shifts with changes in temperature. Fortunately, the dominant effect of temperature transients are shifts of the entire characteristic to higher or lower voltages. Potentially a temperature feedback mechanism can be employed to stabilize the device characteristic.

The amount of modulation for a given change in applied crystal voltage, V_x, was found to vary significantly when V_x is positive as compared with when V_x is negative, i.e.,

$$\Delta I_0 / \Delta V_x \ (V_x > 0) > \Delta I_0 / \Delta V_x \ (V_x < 0),$$

where,

$$V_x = V_a - V_{g2}.$$

A direct consequence of this is, we found that

$$V_x < 0 \rightarrow V_{\lambda/2} = 2.00 kV$$

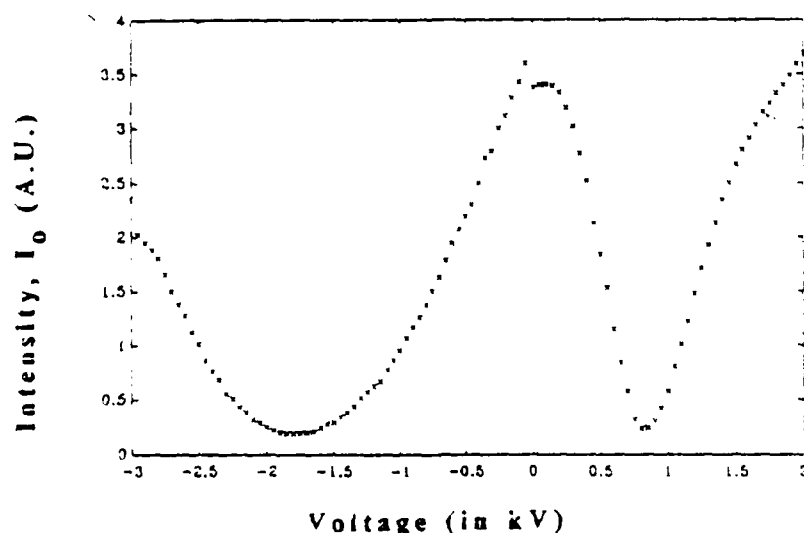$$V_x > 0 \rightarrow V_{\lambda/2} = 0.88 kV.$$

Fig. 11. Voltage/intensity transfer function output intensity as a function of applied crystal voltage.

Two methods were used to obtain the intensity contrast ratio. The first method consisted of writing lines on the modulator that were significantly far apart, and calculating the ratio of maxima and minima. Alternatively, the data generated from the voltage/intensity transfer characteristic was consulted, and the ratio of the maxima and minima computed. Zero in both cases represented the (PMT) output with no light incident on the detector. Intensity contrast ratios of approximately 650:1 were achieved.

Dynamic Crystal Response

The determination of the secondary emission coefficient, δ, of the dielectric mirror on the crystal is of primary importance in understanding the dynamic behavior of the electron beam addressed $LiNbO_3$ phase only spatial phase modulator. Ideally, the maximum charge depletion time for the device will occur when the acceleration potential of the primary electrons is adjusted so that the primary electron energy is near the peak of the collected secondary emission curve of the dielectric mirror. The effective secondary emission coefficient δ' is roughly related to the charge deposition and depletion time via the following formula:

$$\delta' = 1 + t_{deposit}/t_{depletion}$$

The deposition and depletion of charge was accomplished by applying a square waveform to V_a. The half-period of the waveform was sufficiently long to allow the output intensity, I_0, to settle. The amplitude of the square wave was such that when $V_a = V_{low}$, I_0 was at a minimum, I_{min}. When $V_a = V_{\lambda/9}$, I_0 was at an intensity corresponding to $\lambda/9$ modulation depth, $I_{\lambda/9}$. The grid voltage and cathode voltage were adjusted to optimize δ'. In the interest of being able to compare data from run to run, particular care was taken to insure that the same output intensity operating points were maintained. This was achieved by adjusting V_a so that I_{min} and $I_{\lambda/9}$ remained the same when V_k and V_{g2} are changed. The output waveform was recorded on film and the ratio of the 10% - 90% rise time (charge deposition) to 90% - 10% fall time (charge depletion) was calculated. (Fig. 12). The maximum δ' obtained for $-2kV < V_k < -1kV$, $0 < V_{g2} < 1.2kV$ was 2.33. The conditions under which this occurred were, $V_k = -1.5kV$, and $G_2 = 600V$.

$I_{\lambda/9}$

**INTENSITY
(A.U.)**

I_{min}

Time (20 ms/div)

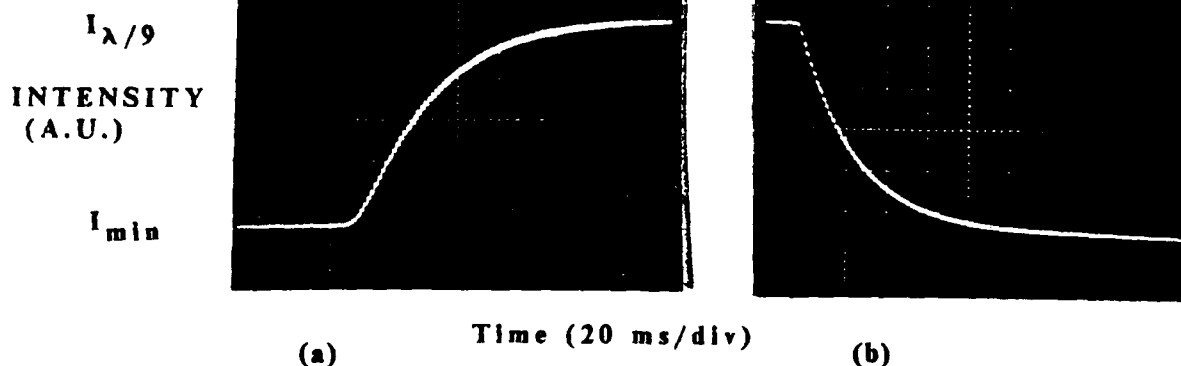(a)   (b)

Fig. 12.   Observation of response times corresponding to the maximum δ achieved with the current 55^0-cut LiNbO$_3$ crystal combined with the ZrO$_2$/SiO$_2$ dielectric mirror. (a) Represents the output intensity in response to charge deposition from crystal surface. (b) Represents the output response to charge depletion from crystal surface.

Framing Speed

A modulator with high framing speed is not essential for the demonstration of programmable phase-only spatial filtering. Because of this, we were able to use a low-current (~1μA), electron gun. For a 330 μm thick 55^0-cut LiNbO$_3$ crystal, the halfwave surface charge density is approximately 0.16μC/cm^2, thus with a 1μA electron beam, we were able to frame in excess of 3 Hz for a 25 mm diameter crystal.

The halfwave framing speed was measured by scanning the entire surface of the crystal with the electron beam so as to generate π radians of phase modulation in a time, $t_{\pi w}$, and then measuring the minimum time, $t_{\pi e}$, required to erase the pattern. The halfwave framing speed given by

$$ f = \frac{1}{t_{\pi e} + t_{\pi w}} $$

Device Ouput Intensity Uniformity

The uniformity of the output intensity of the crystal given a uniform charge distribution across the crystal is a function of the crystal homogeneity, the crystal sensitivity to charge, the grid uniformity, the grid to crystal spacing across the active area of the device, the dielectric mirror uniformity, the laser beam uniformity. Efforts were made to minimize

21

the amount of output intensity nonuniformity contributed by each of these factors.

Device Spatial Resolution

The resolution of a spatial phase modulator is a measure of how much data can be spatially encoded within a single frame. This parameter, together with the cycle time, determines how much data the device is capable of processing per unit time, (i.e., device throughput). The spatial resolution of electrooptic spatial light modulators has been investigated by Roach[10] and by Owechko and Tanguay.[11] For these structures, the resolution has been shown to depend on the dielectric constants and the thicknesses of the various layers. For devices such as the proposed e-beam spatial light modulator and the microchannel spatial light modulators,[12-15] in which a thick, low-dielectric-constant insulating layer (vacuum in this case) separates a thin crystal from an equipotential surface (the grid in this case), the resolution can be shown to be limited by the thickness of the crystal. More specifically, it is the fringing of the electric field within the crystal that limits the resolution. If we consider only the longitudinal component of the electric field, the resolution at the roll-over point on the MTF curve for the e-beam spatial phase modulator is given approximately by

$$N = \frac{1}{\pi l_x} \left(\epsilon_\| / \epsilon_\perp \right)^{1/2}$$

where l_x is the thickness of the crystal, and $\epsilon_\|$ and $\epsilon_\perp$ are the crystal dielectric constants parallel and perpendicular to the longitudinal field respectively. For most electrooptic materials, the transverse electric field components also couple to non-zero electrooptic tensor elements and thus degrades or enhances the spatial resolution from the theoretical value predicted by the above equation. The crystals in the devices observed during the program averaged 330μm thick. Theoretically it should be possible to resolve an average of 3.3 cycles/mm at 50% contrast. Achievement of the thinner crystals was been impeded by the fact that below 330μm the crystals become quite brittle, and break during polishing.

22

The resolution of the device was determined by observing the response in the output intensity of the crystal when a series of line charge distributions of increasing spatial frequency was written to the crystal. Fig 13. The crystal output intensity profile was recorded as a photomultiplier tube, PMT, with a pinhole aperture placed on a motorized translation stage was scanned across the image plane. As the frequency of the line charge distributions were increased the modulation transfer ratio decreases. The spatial resolution is quoted at the 50% contrast. The 'Modulation Transfer Function', 'MTF' was generated from the expression,

$$M T F = \frac{I_{max} - I_{min}}{I_{max} + I_{min}}$$

The quotes are used because strictly speaking MTF curves are generated from sinusoidal line patterns where lines and spaces between lines are of equal width. In our experiments the line charge distributions and the space between the lines was often asymetric. The 'MTF' data indicates that the $ThF_4/SbS_3/LiNbO_3/$Tektronix electron gun combination has a resolution of approximately 1.0 lp/mm at 50% contrast at $V_k = -5.6kV$, $i_{e-beam} = i_{max}$. This 'MTF' value was limited by the resolving power of the Tektronix electron gun and therefore was a representation of the system 'MTF'. Sharp light to dark transition regions have been observed which indicate that the resolving capability of the crystal is much higher. This is also verification that the system is electron gun limited instead of $LiNbO_3$ crystal limited. Further progress on device resolution was curtailed until such a time as an electron gun with a smaller spot was available.
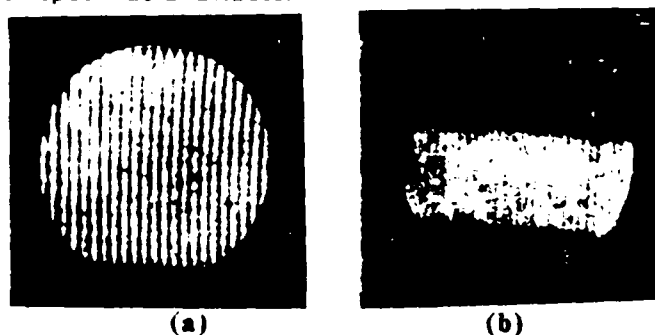

(a)   (b)

Fig. 13.   (a) Photograph of crystal profile. Spatial frequency of lines correspond to 1 lp/mm. Lines written with electrons accelerated at 1.5kV. (b) Spatial frequency = 1.25 lp/mm.

By taking advantage of the storage capability of the SiO_2/ZrO_2 in addition to utilizing an intentionally astigmatic Tektronix electron beam, it was possible to write lines charge distributions at a spatial frequency of 1.0 lp/mm at 65% contrast (V_k = -1.5kV, i_{e-beam} = 100nA/cm), an improvement over the ThF_4/SbS_3 $LiNbO_3$ system. An improvement in system resolution was achieved by adjusting the electron gun spot profile as well as by reducing the electron current. This observation served as conclusive evidence of the resolution limitation imposed by the electron gun.

Phase/Voltage Response and Phase Dynamic Range

The phase dynamic range is determined by the electro-optic coefficients of the crystal, and the breakdown field for the electro-optic plate. It can be shown that the amount of phase delay experienced by the transverse E_x and E_y components of incident radiation transiting an ideal $LiNbO_3$ crystal cut at 55° to the c-axis are:

$\Phi_x(V)$ = 5.84 x 10^{-4} radians/Voit
and,
$\Phi_{-y}(V)$ = 7.27 x 10^{-4} radians/Volt.

When light whose polarization is parallel to one or the other of the crystallographic axes is passed through the crystal, phase retardation will be introduced to that component of the radiation only. It turns out that the largest pure phase modulation can be achieved with 55^{0}-cut $LiNbO_3$ by aligning the input polarization with the -y crystallographic axis. The advantage of using z-cut is that the orientation of the incident polarization is unimportant. This is because the change in index of refraction with voltage is isotropic.

To measure the phase dynamic range, the vacuum-demountable electron-beam-addressed $LiNbO_3$ spatial phase modulator was placed into one arm of a Twyman-Green interferometer. The interferogram indicated that there was a significant curvature of the dielectric mirror with respect to the reference mirror whose flatness was $\lambda/10$. This phenomenon has been observed in other modulators of this type and has been attributed to the concavity arising from the deposition of the ITO layer. To determine the phase dynamic range,

24

the voltage across the crystal was modulated and the output intensity of the central uniform region of the crystal monitored. Amplitude changes in the central fringe arising from changes in applied voltage are related to the introduction of phase retardation/advancement. For light polarized along one of the crystallograhic axes an absolute phase retardation/advancement of 2π was achieved without dielectric breakdown.

A large phase dynamic range would allow a certain degree of compensation for the crystal's nonuniformities to be performed in phase-only filtering applications. It would also allow us to fabricate equipment which could perform beam shaping and steering for the highly divergent output of solid state lasers. Fabrication of a ternary phase-only modulator would also be possible.

Intensity Contrast Ratio

The intensity contrast ratio can also be used to determine the device's amplitude dynamic range. Simply stated, it is the ratio of the maximum output intensity to the minimum output intensity.

Summary of Experimental Results

Tables 1 and 2 summarize the measurements taken on the two directly addressed spatial phase modulators that employed two different dielectric mirrors.

TABLE 1. Performance Parameters for $ThF_4/SbS_3/LiBbO_3$ Combination

Crystal Thickness	$330\mu m$
Storage Time, T_{store}	5 min.
Half-wave Modulation Voltage, $V_{\lambda/2min}$	1000V
Spatial Resolution	1 - 2 lp/mm
Contrast Ratio	20:1
Differential Phase Dynamic Range	5π

TABLE 2. Performance Parameters for $SiO_2/ZrO_2/LiNbO_3$ Combination

Crystal Thickness	$330\mu m$
Storage Time, T_{store}	> 89 hours
Half-wave Modulation Voltage, $V_{\lambda/2min}$	880V
Spatial Resolution	1 - 2 lp/mm
Contrast Ratio	$650 \pm 2.5\%$
Phase Dynamic Range	2π

IV. SEALED-OFF TUBE DEVELOPMENT

Excellent results have been achieved with cold indium sealing techniques. Moderate sucess was achieved with glass fritting techniques. These techniques are well suited for attaching anode/faceplate assemblies to metal/glass vacuum envelopes. The advantage of the Indium sealing process is that the CTP does not have to be subjected to high temperatures from traditional sealing processes, allowing the currently available, less expensive version of the CTP to be used.

A preliminary investigation into the construction of the sealed-off tube version of the device has begun but it's development is outside the scope of the program. One of the advantages of the sealed off version is that a more portable device can be created since no external vacuum pump is needed.

V. CONCLUSIONS

In the program, two prototype anode structures were successfully demonstrated. One anode structure employs Optron's proprietary charge transfer plate (CTP) technology and is the anode of choice for future development of a vacuum-sealed phase-only modulator. The second anode structure employed direct electron-beam-addressing of the crystal and was the primary focus of this program. The anode structure used was a 330um thick $LiNbO_3$ crystal with a theoretical spatial resolution of about 3.3 line pairs/mm. However, the low-resolution electron gun used, with its large spot size, limited the measured spatial resolution to about 1 lp/mm. Nevertheless, framing speeds in excess of 3 Hz, a phase dynamic range of 2π radians, storage times in excess of 90 hours, and a contrast ratio of greater than 650:1 were obtained.

An electron gun with much higher resolution (~100 um spot size) was evaluated during the program but not used to address the anode. Future work on this device should be aimed at using this electron gun to drive the CTP/$LiNbO_3$ anode where the crystal thickness can be reduced to 50um to yield a device with 10 line pairs/mm spatial resolution.

VI. REFERENCES

1. A. Vander Lugt, "Signal Detection by Complex Spatial Filtering," IEEE Trans. Inf. Theory IT-10, 139, 1964.
2. F.T.S. Yu, "Color Image Recognition by Spectral-Spatial Matched Filtering," Opt., Eng., 23, 690-694, 1984.
3. K. Leib, R. Bondurant, S. Hsiao, M Wohlers and R. Herold, "Aerial Reconnaisance Film Screening Using Optical Matched-Filter Correlator Technology," Appl. Opt. 17, 2892, 1978.
4. D. Casasent and A. Furman, "Equalizing and Coherence Measure Correlators," Appl. Opt., 17, 3418, 1978.
5. A. W. Lohmann and D. P. Paris, "Binary Fraunhofer Holograms Generated by Computer," Appl. Opt., 6, 1739, 1967.
6. W. H. Lee, "Binary Computer-Generated Holograms," Appl. Opt., 18, 3661, 1979.
7. J. L. Horner and P. D. Gianino, "Phase-Only Matched Filtering," Appl. Opt., 23, 812, 1984.
8. P. D. Gianino and J.L. Horner, "Additional Properties of the Phase-Only Correlation Filter," Opt. Eng., 23, (6) 695-697, 1984.
9. B. Kazan and M. Knoll, Electrostatic Image Storage, Academic Press, New York, 1968.
10. W.R. Roach, "Resolution of Electro-Optic Light Valves," IEEE Trans. Electron Devices ED-21, 453, 1974.
11. Y. Owechko and A.R. Tanguay, Jr., "Exposure-Induced Charge Distribution Effects on the MTF of Electro-Optic Spatial Light Modulators," Proc. of the SPIE, 218, 67, 1980.
12. C. Warde, A.M. Weiss, A.D. Fisher and J.I. Thackara, "Optical Information Processing Characteristics of the Microchannel Spatial Light Modulator," Appl. Opt., 20, 2066-2074, 1981.
13. C. Warde and J.I. Thackara, "Oblique-cut LiNbO$_3$ Microchannel Spatial Light Modulator," Opt. Lett., 7, 344-346, 1982.
14. C. Warde and J.I. Thackara, "Operating Modes of the Michrochannel Spatial Light Modulator," Opt. Eng., 22 695-702, 1983.
15. A. Schwartz, X-Y. Wang and C. Warde, "Electron-Beam-Addressed Microchannel Spatial Light Modulator," Proc. of the SPIE, 465, 23, 1984.
16. F.M. Dickey and L.A. Romero, "Dual Optimality of the Phase-Only Filter," Optics Letters, 14, 4, 1989.

MISSION
of
Rome Air Development Center

RADC plans and executes research, development, test and selected acquisition programs in support of Command, Control, Communications and Intelligence (C³I) activities. Technical and engineering support within areas of competence is provided to ESD Program Offices (POs) and other ESD elements to perform effective acquisition of C³I systems. The areas of technical competence include communications, command and control, battle management information processing, surveillance sensors, intelligence data collection and handling, solid state sciences, electromagnetics, and propagation, and electronic reliability/maintainability and compatibility.